

\mathcal{PT} -symmetry breaking in quantum spin chains with exceptional non-Hermiticities

Jacob Muldoon and Yogesh N. Joglekar

Department of Physics, Indiana University–Purdue University Indianapolis, Indianapolis, Indiana 46202, USA (Received 3 May 2023; revised 9 October 2023; accepted 16 November 2023; published 6 December 2023)

Since the realization of quantum systems described by non-Hermitian Hamiltonians with parity-time (\mathcal{PT}) symmetry, interest in non-Hermitian, quantum many-body models has steadily grown. Most studies to date map to traditional quantum spin models with a non-Hermiticity that arises from making the model parameters complex or purely imaginary. Here we present a set of models with non-Hermiticity generated by splitting a Hermitian term into two Jordan-normal form parts, and the perturbations are confined to one or two sites. We present exact diagonalization results for a finite \mathcal{PT} threshold in such models and provide an analytical approach for understanding the numerical results. Surprisingly, with non-Hermitian potentials confined to two or even a single site, the \mathcal{PT} threshold seems insensitive to the size of the quantum spin chain. Our results provide a pathway to experimentally feasible non-Hermitian quantum spin chains where the confluence of many-body effects and non-Hermiticity effects can be observed.

DOI: [10.1103/PhysRevA.108.062205](https://doi.org/10.1103/PhysRevA.108.062205)**I. INTRODUCTION**

Since the seminal discovery by Bender *et al.* 25 years ago [1], the field of non-Hermitian systems has dramatically flourished. Research initially focused on continuum, nonrelativistic Schrödinger equations with complex (often purely imaginary) potentials that were invariant under combined operations of parity and time reversal, i.e., $V(x) = V^*(-x)$ [2–4]. Such \mathcal{PT} -symmetric Hamiltonians showed purely real spectra at small non-Hermiticity, going over to complex-conjugate spectra at large non-Hermiticity [5,6]. Experiments in wave systems (optics [7–9], acoustics [10], and the like [11,12]) with balanced, spatially separated gain and loss provided a simple physical interpretation for \mathcal{PT} -symmetric Hamiltonians as effective models for open systems [13,14]. From this vantage point, the \mathcal{PT} -symmetry-breaking transition marks the concomitant emergence of amplifying and decaying modes in an open system. Thus, in the classical domain, \mathcal{PT} -symmetric Hamiltonians are often modeled with purely anti-Hermitian potentials that signify local amplification or absorption. Over the years, these ideas have been generalized to time-periodic models [15–17], non-Markovian models [18,19], and synthetic degrees of freedom [20,21], all in the classical domain.

In the quantum domain, the creation of balanced gain and loss potentials is precluded by thermal fluctuations associated with the dissipation [22] and even at zero temperature the quantum noise associated with linear amplifiers [23,24]. Instead, the coherent nonunitary dynamics generated by \mathcal{PT} -symmetric Hamiltonians is simulated by mode-selective losses [25,26], Hamiltonian dilation [27], or unitary dilation [28] methods. Most recently, it was realized that a Lindbladian minimal quantum system [29–31], when postselected on trajectories that do not undergo quantum jumps [32,33], is described by a non-Hermitian \mathcal{PT} -symmetric Hamiltonian with state-dependent trace-preserving nonlinearity [34]. This technique has enabled the exploration of non-Hermitian Hamiltonians in quantum two-level systems [35–38].

Theoretical studies of non-Hermitian, quantum many-body models have commenced by changing parameters in their Hermitian counterparts from real to complex while maintaining their functional form [39–52]. Such models inherit the symmetries of their Hermitian counterparts, such as translational invariance, and therefore can be analytically investigated. However, preserving those symmetries comes at the cost of having non-Hermitian potentials on a large number of sites, spins, or other relevant degrees of freedom. Experimentally, observing non-Hermitian dynamics in even a single qubit is constrained by an exponentially decaying probability $p_1 \sim e^{-\gamma t}$ for obtaining no-quantum-jump trajectories [35–38]. When simulating the dynamics of a system with n non-Hermitian qubits, the success probability P_n , given by quantum trajectories where none of them undergoes a quantum jump, is doubly exponentially suppressed, $P_n = p_1^n \sim \exp(-n\gamma t)$. This experimental-feasibility analysis endorses a minimal footprint for the non-Hermitian potential, even at the expense of symmetries.

Here we present a class of models with non-Hermiticity created by splitting a Hermitian potential into two Jordan-form terms and then spatially separating them. For example, in a transverse-field quantum Ising model, this means $\gamma \sigma_m^x \rightarrow \gamma(\sigma_{m-n}^+ + \sigma_{m+n}^-)$, where σ_m^α represents the relevant Pauli operator on site m . Note that $\sigma^\pm \equiv (\sigma^x \pm i\sigma^y)/2$ are rank-1 Jordan-form matrices, i.e., they represent single-qubit Hamiltonians at an exceptional point (EP) [35]. Contrary to typical anti-Hermitian potentials, (exceptional) non-Hermiticities such as $\gamma \sigma^\pm$, with their EP degeneracies, do not have an energy scale. In quantum spin systems with a finite number of levels, the mapping between raising (lowering) operators σ^+ (σ^-) and gain (loss) is ambiguous due to the presence of a ceiling in the spectrum. On the contrary, in bosonic models such as two coupled oscillators, this splitting procedure will generate non-Hermitian gain or loss potentials such as $\gamma(a_1^\dagger + a_2)$. We emphasize that the operators σ^\pm are terms in the Hamiltonian, not dissipators routinely used in Lindblad

dynamics to model spontaneous emission and absorption; the latter give rise to anti-Hermitian potentials [53].

In this paper, we investigate the \mathcal{PT} -symmetry-breaking threshold in transverse-field Ising models with a finite number of spins N and its dependence on parameters using an exact diagonalization method. Other traditional techniques such as perturbation theory or tensor networks are ideal for probing a small ground-state-proximate subspace of the exponentially large Hilbert space. Determining the \mathcal{PT} -breaking threshold, where the Hamiltonian first develops complex-conjugate eigenvalues, requires knowledge of the entire spectrum, since the states that develop complex eigenvalues are typically not at the bottom (or the top) of the band [54].

The plan of the paper is as follows. In Sec. II we introduce the canonical quantum Ising chain and its non-Hermitian variations. The non-Hermitian variations on it consist of perturbations on one or two sites. In addition to the \mathcal{PT} threshold for the zero-transverse-field case, we also present the flow of eigenvalues across the \mathcal{PT} -symmetry-breaking transition. In Sec. III we present an analytical approach that explains the surprising insensitivity of the zero-field \mathcal{PT} -threshold results to the spin-chain size N from Sec. II. We conclude the paper in Sec. IV with higher-spin generalizations, a brief feasibility analysis, and a summary. The \mathcal{PT} -threshold results are valid for chains with $N > 2$ where the bulk-vs-edge sites and periodic-vs-open boundary conditions are unambiguously defined but do not seem to depend on N .

II. NON-HERMITIAN QUANTUM ISING MODELS

The canonical quantum Ising model with N sites is described by the Hamiltonian

$$H_0(J, h_z) = -\frac{J}{4} \sum_{i=1}^N \sigma_i^x \sigma_{i+1}^x - \frac{h_z}{2} \sum_{i=1}^N \sigma_i^z, \quad (1)$$

where $J > 0$ is the ferromagnetic coupling between adjacent spins, the uniform transverse field is along the z axis, and the boundary term $\sigma_N^x \sigma_1^x$ is included when periodic boundary conditions are required [55,56]. This exactly solvable model undergoes a quantum phase transition from a spontaneously broken \mathbb{Z}_2 -symmetry phase to a paramagnetic phase with short-range correlations as the transverse-field strength crosses $h_z = J/2$ [57,58].

In this section, we investigate its varied non-Hermitian extensions. We start with the $h_z = 0$ case where H_0 contains only commuting operators and can be trivially diagonalized. Adding a noncommuting term to H_0 changes it into a genuine quantum Ising model.

A. Two-site perturbations with Hermitian or anti-Hermitian limit ($h_z = 0$)

Consider the non-Hermitian extension

$$H_{\text{eff}}(J, h_z | \gamma) = H_0(J, h_z) + \Gamma_{pq}^+(\gamma), \quad (2)$$

$$\Gamma_{pq}^+ = \gamma(\sigma_p^+ + \sigma_q^-) \neq \Gamma_{pq}^{+\dagger}, \quad (3)$$

where $\gamma > 0$ is the strength of the exceptional perturbations σ^\pm and $1 \leq p, q \leq N$ denote their locations along the chain. When $p = q$, the perturbation (3) is trivially Hermitian and the

system has no threshold. Since H_{eff} has real entries, its characteristic polynomial has real coefficients and its eigenvalues are real or complex conjugates [59].

Figure 1 summarizes the \mathcal{PT} -threshold phase diagram of such a quantum spin chain in the absence of transverse field. It involves calculating the spectrum of $H_{\text{eff}}(J, 0 | \gamma)$ by exact diagonalization and then recursively increasing the strength of Γ^+ until complex-conjugate eigenvalues emerge at the threshold $\gamma_{\mathcal{PT}}$. Figure 1(a) shows the dimensionless threshold $\gamma_{\mathcal{PT}}/J$ for an $N = 7$ open chain as a function of (p, q) , but the results remain the same for any chain size $N > 2$. Ignoring the trivial Hermitian case $p = q$ (black diamonds), the threshold results can be grouped into three categories:

$$\gamma_{\mathcal{PT}} = 0 \text{ (red crosses) for adjacent sites } (|p - q| = 1), \quad (4)$$

$$\gamma_{\mathcal{PT}} = J/4 \text{ (blue circles) for edge sites } (|p - q| > 1), \quad (5)$$

$$\gamma_{\mathcal{PT}} = J/2 \text{ (green squares) for bulk sites } (|p - q| > 1). \quad (6)$$

When periodic boundary conditions are imposed on Eq. (1), the ‘‘edge sites’’ category [Eq. (5)] disappears; the threshold is zero when the perturbations σ^\pm are on adjacent sites and $\gamma_{\mathcal{PT}} = J/2$ when they do not share a bond. These numerical results remain unchanged with respect to the number of spins ($N > 2$), (open or periodic) boundary conditions, or the distance $|p - q| \geq 2$ and the locations of the two sites along the chain. This surprising nonzero threshold implies that the \mathcal{P} operator is not the spatial reflection, $k \leftrightarrow N + 1 - k$. Indeed, since the Hamiltonian $H_{\text{eff}}(J, h_z | \gamma)$ is purely real, its antilinear symmetry can be chosen as $\mathcal{P} = \mathbb{1}_N$ and $\mathcal{T} = *$ (complex conjugation).

To understand the mechanism of \mathcal{PT} -symmetry breaking under exceptional perturbations, we show the flow of eigenvalues $\text{Re}(E)$ (blue lines) and $\text{Im}(E)$ (red lines) as a function of γ/J in Figs. 1(b)–1(f). Since the eigenvalues occur in complex-conjugate pairs, it is sufficient to plot $\text{Im}(E) > 0$. When the potentials are maximally separated $(p, q) = (1, N)$, starting from N bands with varying degeneracies, a set of central bands undergoes level attraction and develops imaginary parts at $\gamma = J/4$ [Fig. 1(b)]. The ground state (or its particle-hole symmetric counterpart) does not participate in \mathcal{PT} -symmetry breaking. Figure 1(c), with $(p, q) = (6, 4)$, shows that for bulk nonadjacent sites, again, \mathcal{PT} symmetry breaks with a multitude of bands across the energy-level spectrum at $\gamma = J/2$. The trivial case of a Hermitian perturbation $p = 1 = q$ shows expected linear level splitting [Fig. 1(d)]. When the perturbation sites share a bond, $(p, q) = (2, 1)$, linearly increasing $\text{Im}(E)$ signals the zero threshold [Fig. 1(e)]. We note that the bands developing complex eigenvalues are neither particle-hole symmetric nor at the bottom or the top. Finally, when the edge perturbation sites are not maximally separated, $(p, q) = (6, 1)$, the flow of eigenvalues is different [Fig. 1(f)] from the results in Fig. 1(a).

Next we replace the Γ_{pq}^+ potential by

$$\Gamma_{pq}^- = \gamma(\sigma_p^+ - \sigma_q^-), \quad (7)$$

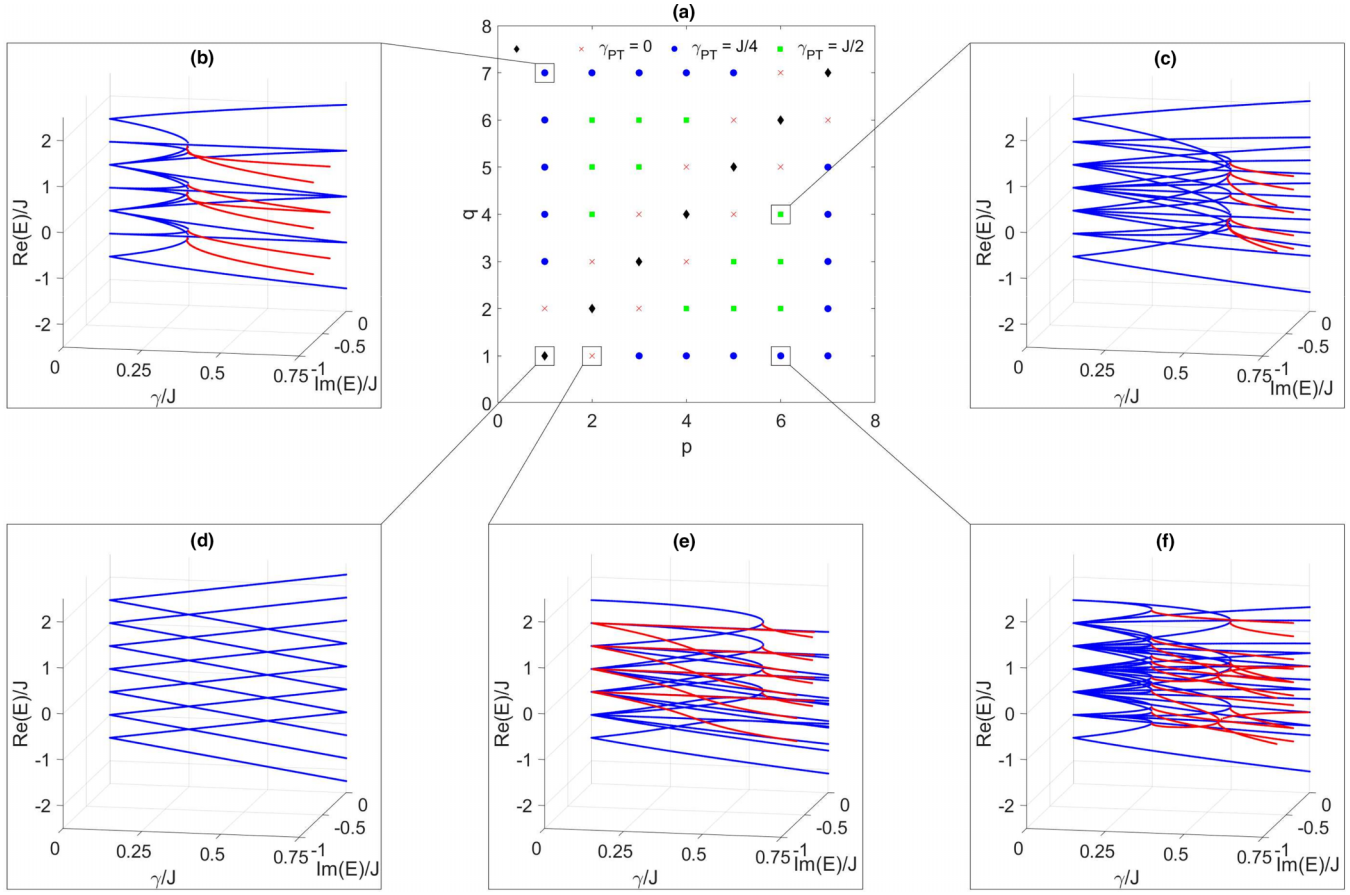


FIG. 1. \mathcal{PT} -breaking threshold for a seven-spin chain with $h_z = 0$ and non-Hermiticity $\Gamma_{p,q}^+$ [Eq. (3)]. (a) Apart from the Hermitian case at $p = q$ (black diamonds), the threshold takes three possible values: zero for adjacent sites (red crosses), $\gamma_{\mathcal{PT}}(p, q) = J/4$ when at least one site is at the edge (blue circles), and $\gamma_{\mathcal{PT}}(p, q) = J/2$ when both sites are in the bulk (green squares). (b)–(f) Flow of eigenvalues $\text{Re}(E)(\gamma)/J$ [blue (dark gray) lines, bound to the real plane] and $\text{Im}(E)(\gamma)/J > 0$ [red (light gray) lines, protruding forward] for the (p, q) locations marked in (a). At $\gamma = 0$, the system has seven particle-hole symmetric bands with varying degeneracies spanning the $2^7 = 128$ eigenvalues; at a finite γ , the particle-hole symmetry is generally broken. The ground-state band typically does not participate in the \mathcal{PT} -symmetry-breaking transition. Therefore, variational or perturbative methods that focus on the lowest-lying states cannot be used to determine the \mathcal{PT} -symmetry-breaking threshold.

which reduces to an anti-Hermitian term $\Gamma_{pp}^- = i\gamma\sigma_y$ when $p = q$. When $p \neq q$, the \mathcal{PT} threshold $\gamma_{\mathcal{PT}}(p, q) = \gamma_{\mathcal{PT}}(q, p)$ is given by Eqs. (4)–(6). When $p = q$, the resulting threshold $\gamma_{\mathcal{PT}}(p, p) = 0$ for a bulk site, whereas $\gamma_{\mathcal{PT}} = J/4$ for an edge site. The \mathcal{PT} thresholds obtained from exact diagonalization appear to be independent of the number of spins $N > 2$, the distance $|p - q| > 1$ between the perturbations, and the nature of boundary conditions. Here too, since Eq. (7) has purely real entries, $\mathcal{PT} = \mathbb{1}_N^*$ gives the corresponding antilinear symmetry.

The simple expressions for the \mathcal{PT} threshold [Eqs. (4)–(6)] hint at an analytical solution. At this point, it is important to recall that the spectrum of the Hamiltonian (1) is traditionally obtained by using the Jordan-Wigner transformation to map the problem onto noninteracting fermions [57,58]. Under this mapping, however, the exceptional perturbations σ_p^+ and σ_q^- create non-Hermitian, fermionic string operators, thereby rendering such an approach useless.

B. Single-site perturbations ($h_z = 0$)

Inspired by the repeating structure of bands in Fig. 1 and the finite \mathcal{PT} threshold obtained in the anti-Hermitian limit of Eq. (7), we now consider the Ising spin chain with a single-site perturbation

$$\Gamma_p(\gamma_+, \gamma_-) = \gamma_+\sigma_p^+ + \gamma_-\sigma_p^-, \quad (8)$$

where $\gamma_{\pm} \in \mathbb{R}$ denote the strengths of (exceptional) non-Hermiticities σ_p^{\pm} that act on the spin at site p . Starting with the case $\gamma_- = 0$, the \mathcal{PT} -breaking threshold for the Hamiltonian $H_0 + \Gamma_p(\gamma, 0)$ is given by

$$\gamma_{\mathcal{PT}}(p) = \begin{cases} J/4 & \text{for the edge case} \\ J/2 & \text{for the bulk case.} \end{cases} \quad (9)$$

Figure 2 shows the evolution of the energy spectra of an $N = 8$ chain as a function of γ when the sole perturbation σ^+ is on the edge site [Fig. 2(a)] and the bulk site $p = 2$

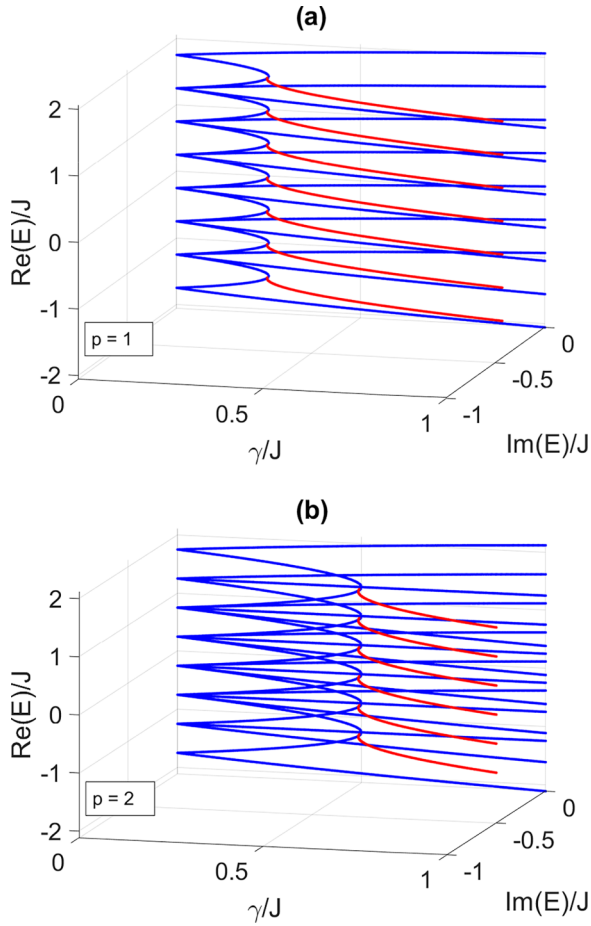


FIG. 2. Flow of eigenvalues $E(\gamma)/J$ for an eight-spin chain with potential $\gamma\sigma^+$ on one site. Blue (dark gray) lines (bound to the real plane) are used for $E(\gamma)/J$ that are purely real and red (light gray) lines (protruding forward) are used for $E(\gamma)/J$ that have an imaginary part. At $\gamma = 0$, the system has eight particle-hole symmetric bands with varying degeneracies that account for the total $2^8 = 256$ eigenvalues. (a) When the site is at the edge, $\text{Im}(E) > 0$ emerge past the threshold $\gamma_{\text{PT}} = J/4$. (b) For a bulk site $p = 3$, the complex-conjugate eigenvalues occur past the threshold $\gamma_{\text{PT}} = J/2$.

[Fig. 2(b)]. These results have many features in common with the eigenvalue flows in Fig. 1. Specifically, we see that starting with N particle-hole symmetric bands at $\gamma = 0$, the \mathcal{PT} breaking occurs at a threshold equal to $J/4$ or $J/2$, respectively, but the ground-state eigenvalue does not become complex. Since a unitary basis change can map $\sigma_y \rightarrow -\sigma_y$ without changing the interaction term in H_0 [Eq. (1)], the threshold results for a $\Gamma_p(0, \gamma)$ perturbation are the same as in Eq. (9).

Finally, we consider the case where both γ_{\pm} are varied. The non-Hermitian purely real Hamiltonian is given by

$$H_{\text{eff}} = H_0 + (\gamma_+ + \gamma_-)\sigma_p^x + i(\gamma_+ - \gamma_-)\sigma_p^y. \quad (10)$$

We characterize the \mathcal{PT} -phase diagram in the (γ_+, γ_-) plane by plotting the largest imaginary part of the eigenvalues of $H_{\text{eff}}(\gamma_+, \gamma_-)$ obtained via exact diagonalization (Fig. 3). It

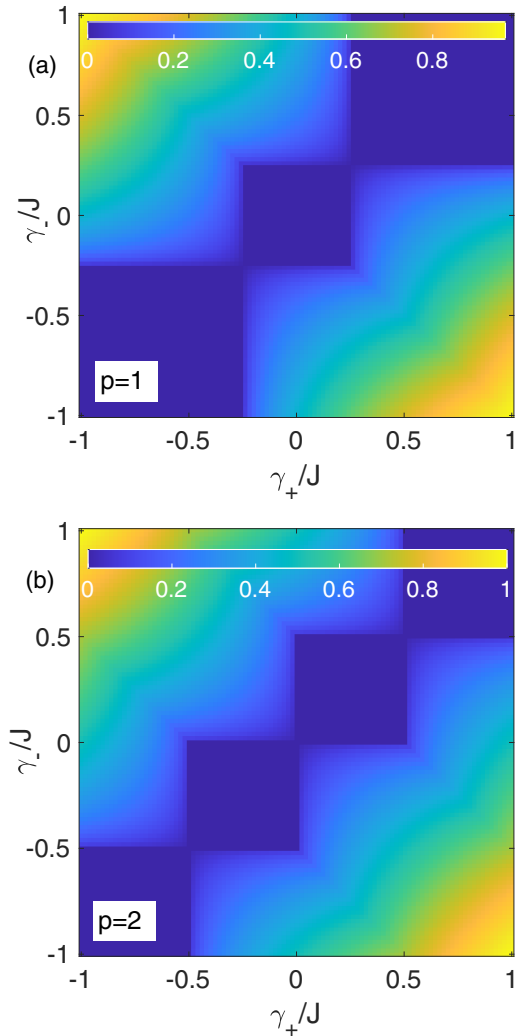


FIG. 3. \mathcal{PT} -phase diagram of a six-spin chain in the (γ_+, γ_-) plane. Color denotes the maximum imaginary part $\text{Im}(E)/J$ of the eigenvalues of the Hamiltonian (10). Deep blue regions indicate the \mathcal{PT} -symmetric phase. (a) When the perturbation site is at the edge ($p = 1$), γ_{PT} is positive along the antidiagonal. (b) When the site is in the bulk ($p = 2$), the threshold is zero.

indicates whether the system is in the \mathcal{PT} -symmetric phase $\max \text{Im}(E) = 0$ (deep blue) or \mathcal{PT} -symmetry-broken phase $\max \text{Im}(E) > 0$ (other colors) and quantifies the amplification rate for the \mathcal{PT} -broken eigenstates. Along the diagonal $\gamma_+ = \gamma_-$, H_{eff} is Hermitian and the spectrum is always real. Along the other diagonal, given by $\gamma_+ + \gamma_- = 0$, the perturbation (8) is anti-Hermitian. In this case, we obtain a positive threshold for the edge case [Fig. 3(a)], while the threshold is zero for the bulk case [Fig. 3(b)], as seen in Sec. II A.

The \mathcal{PT} -phase diagram in Fig. 3 is symmetric under individual reflections across the two diagonals. Since $\text{Im}(E)(\gamma_+, \gamma_-)$ is an even function of the strength of the $i\sigma^y$ term in Eq. (10), reflection symmetry along the main diagonal is expected. Reflection symmetry along the antidiagonal, on the other hand, arises because the Hermitian term in Γ_p [Eq. (8)] commutes with the Ising interaction term H_0 .

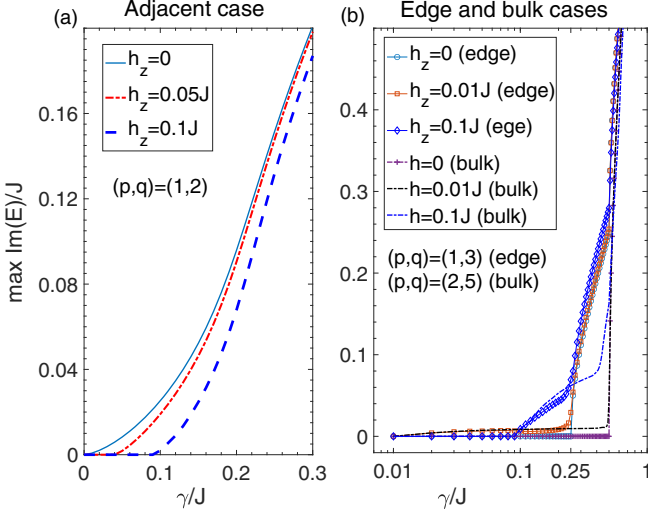


FIG. 4. Threshold $\gamma_{\mathcal{PT}}(h_z)$ for the Hamiltonian (2) with $N = 9$ spins and exceptional perturbations on two sites. (a) For perturbation Γ_{pq}^+ , adjacent sites with zero threshold develop a finite threshold proportional to $|h_z|$. This is signified by $\max \text{Im}(E) = 0$ regions that emerge at small γ when $h_z \neq 0$. (b) For edge sites, the $h_z = 0$ threshold at $\gamma/J = 0.25$ [Eq. (5)] is suppressed to vanishingly small values when $h_z = 0^+$ and increases with h_z thereafter (solid lines with symbols). For bulk sites, the threshold at $\gamma/J = 0.5$ [Eq. (6)] is also suppressed to zero for $h_z = 0^+$ and increases with h_z (dot-dashed lines).

C. Effect of nonzero transverse field on two-site perturbations ($h_z \neq 0$)

When the transverse field h_z is introduced, the Hamiltonian H_{eff} contains three mutually noncommuting pieces, one for each Pauli matrix. Since the \mathcal{PT} -threshold results depend only on h_z , without loss of generality, we choose $h_z > 0$. Here we consider the fate of the Hamiltonian (2) where potentials σ^\pm are introduced on sites p and q , respectively. Apart from the trivial Hermitian case ($p = q$), the behavior of the threshold $\gamma_{\mathcal{PT}}$ can be categorized as

$$\gamma_{\mathcal{PT}}(h_z) = A_1 h_z \quad \text{for adjacent sites,} \quad (11)$$

$$\gamma_{\mathcal{PT}}(h_z) = (J/4) + A_2 h_z \quad \text{for both edge sites,} \quad (12)$$

$$\gamma_{\mathcal{PT}}(h_z) = (J/4)\delta_{h,0} + A_3 h_z \quad \text{for one edge site,} \quad (13)$$

$$\gamma_{\mathcal{PT}}(h_z) = (J/2)\delta_{h,0} + A_4 h_z \quad \text{for bulk sites,} \quad (14)$$

where A_k are configuration-dependent parameters. This behavior also persists when the non-Hermitian perturbation is changed to $\Gamma'_{pq}(\gamma) \equiv \gamma(\sigma_p^+ + \sigma_q^+)$.

Figure 4 shows the typical dependence of $\max \text{Im}(E)(\gamma)$ on the transverse field h_z for the Hamiltonian $H_{\text{eff}} = H_0 + \Gamma_{pq}^+$. For adjacent sites $p = q \pm 1$, the zero threshold at $h_z = 0$ is lifted to values proportional to h_z . This is indicated by broadening of the region where $\max \text{Im}(E) = 0$ as γ is increased from zero [Fig. 4(a)]. For nonadjacent cases, if one of the sites is at the edge, the $h_z = 0$ threshold is given by $\gamma_{\mathcal{PT}} = J/4$. It is suppressed to zero with the introduction of the transverse field. As h_z increases, the threshold also increases.

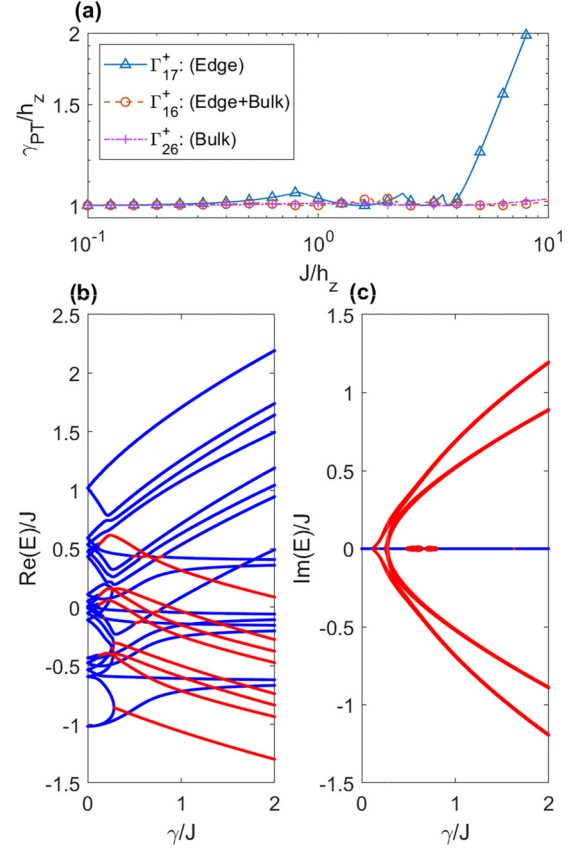


FIG. 5. (a) Threshold $\gamma_{\mathcal{PT}}(h_z)$ for the Hamiltonian (2) with $N = 7$ spins, now normalized vs the transverse field h_z . Though the threshold $\gamma_{\mathcal{PT}}(h_z)$ depends on the exact values of p, q, J , and h_z , it is never less than h_z . Also shown is the flow of eigenvalues (b) $\text{Re}(E)(\gamma/J)$ [blue (dark gray)] and (c) $\text{Im}(E)(\gamma/J)$ [red (light gray)] for an $N = 5$ spin chain with perturbation Γ_{12}^- at transverse field $h_z/J = 0.1$. The eigenvalues become complex conjugates in three distinct groups. The imaginary parts of the first two groups grow with increasing γ , whereas the third group shows recombinant behavior where pairs of eigenvalues become complex conjugates and then real again with increasing γ/J . The \mathcal{PT} threshold, defined by the first emergence of complex eigenvalues, is dependent on p, q, J , and h_z .

Similar behavior is observed for $\max \text{Im}(E)(\gamma)$ when both sites are in the bulk [Fig. 4(b)]. We have verified that these results hold for spin chains up to size $N = 12$.

Next we consider the threshold in the weak-coupling limit $J \ll h_z, \gamma$, where the Hamiltonian becomes

$$H \approx -\frac{h_z}{2} \sum_{i=1} \sigma_i^z + \gamma(\sigma_p^+ + \sigma_q^-). \quad (15)$$

Since the perturbations $\gamma\sigma^\pm = \gamma\sigma^x \pm i\gamma\sigma^y$ are already at the EP, adding a nonzero Hermitian transverse field displaces the EP eigenvalues onto the real axis $0 = \sqrt{\gamma^2 + (i\gamma)^2} \rightarrow \pm|h_z|/2$. Therefore, in the limit $J \rightarrow 0$, the \mathcal{PT} threshold for Eq. (15) diverges. For intermediate values of J/h_z , we find that the threshold remains finite $\gamma_{\mathcal{PT}} \sim h_z$, albeit dependent on the configuration. Figure 5(a) shows this behavior through (representative) results for an $N = 7$ spin chain with configurations listed in (12)–(14). Figure 5(b) shows the eigenvalue flows for $h_z = J$ as a function of γ . The particle-hole symmetry of the

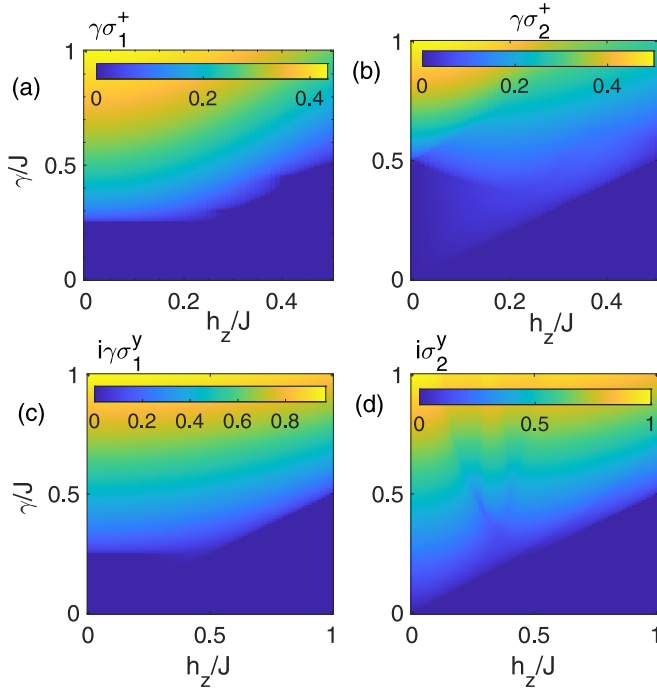


FIG. 6. Evolution of $\max \text{Im}(E)(\gamma, h_z)$ of the Hamiltonian (10) with $N = 7$ spins. Deep blue regions [$\max \text{Im}(E) = 0$] indicate \mathcal{PT} -symmetric phase. (a) For edge-site perturbation $\gamma\sigma_1^+$, the threshold increases from $J/4$ with increasing h_z . (b) For the same perturbation in the bulk, the threshold increases from $\gamma_{\mathcal{PT}}(h = 0^+) = 0$ while its value is $J/2$ at $h_z = 0$. (c) Same as (a) but for anti-Hermitian edge perturbation. (d) Same as (b) but for anti-Hermitian bulk-site perturbation, where the no-field threshold is zero.

spectrum in Fig. 1 is destroyed by a nonzero transverse field, the degeneracies are also lifted, and complex eigenvalues now occur at different values of γ for different sets of levels.

D. Effect of nonzero transverse field on single-site perturbation ($h_z \neq 0$)

Finally, we investigate the h_z dependence of $\gamma_{\mathcal{PT}}$ for the single-site perturbation model (10) with $\gamma_- = 0$, by tracking the maximum imaginary part of its eigenvalues, $\max \text{Im}(E)(\gamma, h_z)$. Figure 6(a) shows that for an edge perturbation, starting from $J/4$, the threshold continuously increases with h_z . In contrast, when the exceptional potential $\gamma\sigma^+$ is on an interior site, the threshold $J/2$ at $h_z = 0$ is suppressed to vanishingly small values for $h_z \rightarrow 0$ before increasing linearly with h_z [Fig. 6(b)]. When the edge-site potential is purely anti-Hermitian, starting from $J/4$, the threshold further increases continuously with h_z [Fig. 6(c)]. Figure 6(d) shows that when the anti-Hermitian potential $i\gamma\sigma^y$ is in the bulk, the zero threshold at $h_z = 0$ is linearly lifted. Thus, the transverse field can strengthen or weaken the \mathcal{PT} -symmetric phase.

III. SYMMETRIES AND THE \mathcal{PT} -BREAKING THRESHOLD

The simple N -independent results for the \mathcal{PT} -breaking threshold for a quantum Ising chain in the absence of

a transverse field hint at an analytical solution. The numerically observed stability of that threshold $\gamma_{\mathcal{PT}}$ in the points to the possibility of investigating the interplay between the h_z/J -driven quantum phase transition and the γ/J -driven \mathcal{PT} -symmetry-breaking transition. Here we discuss the analytical solution that shows why the \mathcal{PT} threshold is robust when $h_z = 0$.

Consider the zero-field model with a single-site perturbation $\Gamma_p(\gamma, 0)$ [Eq. (8)]. The eigenstates of H_0 [Eq. (1)] can be written as $|\psi\rangle = |\pm_1\rangle \otimes |\pm_2\rangle \cdots |\pm_N\rangle$, where $\sigma_m^x|\pm_m\rangle = \pm|\pm_m\rangle$ are the symmetric (antisymmetric) eigenstates at site m . For a perturbation on site p , we consider an eigenstate ansatz as

$$|\phi\rangle \equiv |\pm_1\rangle \cdots |\hat{n}_p\rangle \cdots |\pm_N\rangle, \quad (16)$$

where $|\hat{n}_p\rangle$ denotes the spin state at the perturbation site. The eigenvalue equation satisfied by the state $|\phi\rangle$ becomes

$$H_p|\hat{n}_p\rangle = \left(h_x\sigma^x + i\frac{\gamma}{2}\sigma^y\right)|\hat{n}_p\rangle = E_p|\hat{n}_p\rangle, \quad (17)$$

$$h_x = -\frac{J}{4}\langle\phi|\sigma_{p-1}^x + \sigma_{p+1}^x|\phi\rangle + \frac{\gamma}{2}, \quad (18)$$

where one of the $p \pm 1$ terms is absent when the location p is at the edge. The 2×2 Hamiltonian H_p [Eq. (17)] undergoes \mathcal{PT} -symmetry breaking when the strength of the imaginary field is equal to that of the real field, i.e., $h_x = \pm\gamma/2$. This gives Eq. (9) as the threshold result. A similar analysis can be carried out for other exceptional potentials, including two-site potentials [Eq. (3)], when the two sites are not adjacent. When the two sites are adjacent, a similar reduction to a 4×4 Hamiltonian gives the zero threshold [Eq. (4)]. The interaction contribution to the effective field in Eq. (18) vanishes in states where the neighboring spins $p \pm 1$ have opposite projections. For such states, the effective Hamiltonian H_p remains at the exceptional point, producing γ -independent flat bands in the energy spectrum that never become complex. This unusual behavior results solely from our choice of exceptional non-Hermiticities $\gamma\sigma^\pm$ that generate no energy scale.

It is a useful exercise to think about what the threshold analysis presented here would look like in the Jordan-Wigner fermions language. When $h_z = 0$, the single- or two-site non-Hermiticities will lead to (p, q) -dependent fermionic strings, all of which lead to simple threshold answers. One might imagine obtaining different energy shifts through a perturbative analysis. However, it is known that the perturbation theory cannot be used to predict the \mathcal{PT} threshold as its radius of convergence is exactly at the boundary between the \mathcal{PT} -symmetric and \mathcal{PT} -symmetry-broken regions [60,61]. Adding a transverse field h_z only changes the fermions that diagonalize the Hermitian Hamiltonian through a Bogoliubov transform. Thus, the relative insensitivity of the threshold $\gamma_{\mathcal{PT}}$ to configuration details is a common feature of systems with or without the transverse field.

Note that although the two-site perturbation was motivated by splitting a Hermitian term into two Jordan-normal-form terms, symmetries in the $h_z = 0$ case map $\sigma^+ \leftrightarrow \sigma^-$ under a local unitary transformation on the site of the potential. This equivalence between the two potentials is another reminder

that in systems with a bounded eigenvalue spectrum, “gain” and “loss” are not equivalent to raising and lowering operators. Additional unitary-equivalent terms such as $\gamma\sigma^+ \leftrightarrow -\gamma\sigma^+$ or $h_z \leftrightarrow -h_z$ were already taken into account when obtaining the \mathcal{PT} -threshold results.

IV. DISCUSSION

In this paper, we have developed a class of \mathcal{PT} -symmetric quantum Ising models with N spins, where the non-Hermitian potentials are confined to one or two sites and the resulting nonzero \mathcal{PT} threshold appears to be independent of $N > 2$. In most traditional models, the non-Hermiticity is introduced by changing model parameters from real to complex. That means the number of sites with non-Hermiticity is proportional to N , something that is virtually impossible to implement in coupled-qubit realizations of a quantum spin chain. Therefore, with experimental feasibility in mind, we have chosen localized non-Hermiticities. Our second deliberate choice is that instead of commonly used anti-Hermitian potentials (obtained by changing a parameter from real to purely imaginary), we have used perturbations that by themselves do not generate an

energy scale and therefore keep the system at an EP in the limit $\gamma \gg J, h_z$.

Our models show that introducing a single non-Hermitian qubit in a Hermitian quantum Ising chain gives rise to a $\gamma_{\mathcal{PT}}$ that can be varied with the transverse field. With full control required over only the non-Hermitian qubit, our models provide a pathway to investigate the interplay between interaction and non-Hermitian properties. Our results remain qualitatively unchanged when the Hermitian Hamiltonian is changed from a quantum Ising model to its integer-spin counterpart or Heisenberg model with or without anisotropies. The spin-1 case, for example, is made richer by the possibility of different exceptional perturbations such as $S^+ = (S^x + iS^y)/2$ and $S^{+2} \neq 0$. An exact diagonalization analysis is required to obtain the general threshold $\gamma_{\mathcal{PT}}(J_{xx}, J_{yy}, J_{zz}; \mathbf{h})$ as a function of the multiple, possible non-Hermiticities, and its exhaustive characterization is an open problem.

ACKNOWLEDGMENT

This work was supported by ONR Grant No. N00014-21-1-2630. We thank P. Durganandini and K. Murch for discussions.

-
- [1] C. M. Bender and S. Boettcher, Real spectra in non-Hermitian Hamiltonians having \mathcal{PT} symmetry, *Phys. Rev. Lett.* **80**, 5243 (1998).
 - [2] C. M. Bender, D. C. Brody, and H. F. Jones, Complex extension of quantum mechanics, *Phys. Rev. Lett.* **89**, 270401 (2002).
 - [3] A. Mostafazadeh, Pseudo-Hermiticity versus \mathcal{PT} symmetry: The necessary condition for the reality of the spectrum of a non-Hermitian Hamiltonian, *J. Math. Phys.* **43**, 205 (2002).
 - [4] A. Mostafazadeh, Exact \mathcal{PT} -symmetry is equivalent to Hermiticity, *J. Phys. A: Math. Gen.* **36**, 7081 (2003).
 - [5] C. M. Bender, Making sense of non-Hermitian Hamiltonians, *Rep. Prog. Phys.* **70**, 947 (2007).
 - [6] Y. N. Joglekar, C. Thompson, D. D. Scott, and G. Vemuri, Optical waveguide arrays: Quantum effects and \mathcal{PT} symmetry breaking, *Eur. Phys. J. Appl. Phys.* **63**, 30001 (2013).
 - [7] A. Guo, G. J. Salamo, D. Duchesne, R. Morandotti, M. Volatier-Ravat, V. Aimez, G. A. Siviloglou, and D. N. Christodoulides, Observation of \mathcal{PT} -symmetry breaking in complex optical potentials, *Phys. Rev. Lett.* **103**, 093902 (2009).
 - [8] C. E. Rüter, K. G. Makris, R. El-Ganainy, D. N. Christodoulides, M. Segev, and D. Kip, Observation of parity-time symmetry in optics, *Nat. Phys.* **6**, 192 (2010).
 - [9] A. Regensburger, C. Bersch, M.-A. Miri, G. Onishchukov, D. N. Christodoulides, and U. Peschel, Parity-time synthetic photonic lattices, *Nature (London)* **488**, 167 (2012).
 - [10] X. Zhu, H. Ramezani, C. Shi, J. Zhu, and X. Zhang, \mathcal{PT} -symmetric acoustics, *Phys. Rev. X* **4**, 031042 (2014).
 - [11] B. Peng, Ş. K. Özdemir, F. Lei, F. Monifi, M. Gianfreda, G. L. Long, S. Fan, F. Nori, C. M. Bender, and L. Yang, Parity-time-symmetric whispering-gallery microcavities, *Nat. Phys.* **10**, 394 (2014).
 - [12] H. Hodaei, M.-A. Miri, M. Heinrich, D. N. Christodoulides, and M. Khajavikhan, Parity-time-symmetric microring lasers, *Science* **346**, 975 (2014).
 - [13] J. Schindler, A. Li, M. C. Zheng, F. M. Ellis, and T. Kottos, Experimental study of active LRC circuits with \mathcal{PT} symmetries, *Phys. Rev. A* **84**, 040101(R) (2011).
 - [14] C. M. Bender, B. K. Berntson, D. Parker, and E. Samuel, Observation of \mathcal{PT} phase transition in a simple mechanical system, *Am. J. Phys.* **81**, 173 (2013).
 - [15] Y. N. Joglekar, R. Marathe, P. Durganandini, and R. K. Pathak, \mathcal{PT} spectroscopy of the Rabi problem, *Phys. Rev. A* **90**, 040101(R) (2014).
 - [16] M. Chitsazi, H. Li, F. M. Ellis, and T. Kottos, Experimental realization of Floquet \mathcal{PT} -symmetric systems, *Phys. Rev. Lett.* **119**, 093901 (2017).
 - [17] M. A. Quiroz-Juárez, K. S. Agarwal, Z. A. Cochran, J. L. Aragón, Y. N. Joglekar, and R. de J. León-Montiel, On-demand parity-time symmetry in a lone oscillator through complex synthetic gauge fields, *Phys. Rev. Appl.* **18**, 054034 (2022).
 - [18] Z. A. Cochran, A. Saxena, and Y. N. Joglekar, Parity-time symmetric systems with memory, *Phys. Rev. Res.* **3**, 013135 (2021).
 - [19] A. Wilkey, G. Vemuri, and Y. N. Joglekar, in *Active Photonic Platforms XII*, edited by G. S. Subramania and S. Foteinopoulou (SPIE, Bellingham, 2020).
 - [20] J. Zhang, L. Li, G. Wang, X. Feng, B.-O. Guan, and J. Yao, Parity-time symmetry in wavelength space within a single spatial resonator, *Nat. Commun.* **11**, 3217 (2020).
 - [21] Q. Ding, M. Wang, J. Zhang, Y. Tang, Y. Li, M. Han, Y. Guo, N. Zhang, B. Wu, and F. Yan, Parity-time symmetry in parameter space of polarization, *APL Photon.* **6**, 076102 (2021).
 - [22] R. Kubo, The fluctuation-dissipation theorem, *Rep. Prog. Phys.* **29**, 255 (1966).
 - [23] C. M. Caves, Quantum limits on noise in linear amplifiers, *Phys. Rev. D* **26**, 1817 (1982).

- [24] S. Scheel and A. Szameit, \mathcal{PT} -symmetric photonic quantum systems with gain and loss do not exist, *Europhys. Lett.* **122**, 34001 (2018).
- [25] L. Xiao, X. Zhan, Z. H. Bian, K. K. Wang, X. Zhang, X. P. Wang, J. Li, K. Mochizuki, D. Kim, N. Kawakami, W. Yi, H. Obuse, B. C. Sanders, and P. Xue, Observation of topological edge states in parity-time-symmetric quantum walks, *Nat. Phys.* **13**, 1117 (2017).
- [26] J. Li, A. K. Harter, J. Liu, L. de Melo, Y. N. Joglekar, and L. Luo, Observation of parity-time symmetry breaking transitions in a dissipative Floquet system of ultracold atoms, *Nat. Commun.* **10**, 855 (2019).
- [27] Y. Wu, W. Liu, J. Geng, X. Song, X. Ye, C.-K. Duan, X. Rong, and J. Du, Observation of parity-time symmetry breaking in a single-spin system, *Science* **364**, 878 (2019).
- [28] N. Maraviglia, P. Yard, R. Wakefield, J. Carolan, C. Sparrow, L. Chakhmakhchyan, C. Harrold, T. Hashimoto, N. Matsuda, A. K. Harter, Y. N. Joglekar, and A. Laing, Photonic quantum simulations of coupled \mathcal{PT} -symmetric Hamiltonians, *Phys. Rev. Res.* **4**, 013051 (2022).
- [29] G. Lindblad, On the generators of quantum dynamical semigroups, *Commun. Math. Phys.* **48**, 119 (1976).
- [30] V. Gorini, A. Kossakowski, and E. Sudarshan, Completely positive dynamical semigroups of N -level systems, *J. Math. Phys.* **17**, 821 (1976).
- [31] D. Manzano, A short introduction to the Lindblad master equation, *AIP Adv.* **10**, 025106 (2020).
- [32] K. Mølmer, Y. Castin, and J. Dalibard, Monte Carlo wavefunction method in quantum optics, *J. Opt. Soc. Am. B* **10**, 524 (1993).
- [33] F. Minganti, A. Miranowicz, R. W. Chhajlany, and F. Nori, Quantum exceptional points of non-Hermitian Hamiltonians and Liouvillians: The effects of quantum jumps, *Phys. Rev. A* **100**, 062131 (2019).
- [34] D. C. Brody and E.-M. Graefe, Mixed-state evolution in the presence of gain and loss, *Phys. Rev. Lett.* **109**, 230405 (2012).
- [35] M. Naghiloo, M. Abbasi, Y. N. Joglekar, and K. W. Murch, Quantum state tomography across the exceptional point in a single dissipative qubit, *Nat. Phys.* **15**, 1232 (2019).
- [36] F. Klauck, L. Teuber, M. Ornigotti, M. Heinrich, S. Scheel, and A. Szameit, Observation of \mathcal{PT} -symmetric quantum interference, *Nat. Photon.* **13**, 883 (2019).
- [37] L. Ding, K. Shi, Q. Zhang, D. Shen, X. Zhang, and W. Zhang, Experimental determination of \mathcal{PT} -symmetric exceptional points in a single trapped ion, *Phys. Rev. Lett.* **126**, 083604 (2021).
- [38] A. Quinn, J. Metzner, J. E. Muldoon, I. D. Moore, S. Brudney, S. Das, D. T. C. Allcock, and Y. N. Joglekar, Observing super-quantum correlations across the exceptional point in a single, two-level trapped ion, [arXiv:2304.12413](https://arxiv.org/abs/2304.12413).
- [39] C. Korff, \mathcal{PT} symmetry of the non-Hermitian XX spin-chain: Non-local bulk interaction from complex boundary fields, *J. Phys. A: Math. Theor.* **41**, 295206 (2008).
- [40] O. A. Castro-Alvaredo and A. Fring, A spin chain model with non-Hermitian interaction: The Ising quantum spin chain in an imaginary field, *J. Phys. A: Math. Theor.* **42**, 465211 (2009).
- [41] T. Deguchi and P. K. Ghosh, The exactly solvable quasi-hermitian transverse Ising model, *J. Phys. A: Math. Theor.* **42**, 475208 (2009).
- [42] Y. Ashida, S. Furukawa, and M. Ueda, Parity-time-symmetric quantum critical phenomena, *Nat. Commun.* **8**, 15791 (2017).
- [43] K. Yamamoto, M. Nakagawa, K. Adachi, K. Takasan, M. Ueda, and N. Kawakami, Theory of non-Hermitian fermionic superfluidity with a complex-valued interaction, *Phys. Rev. Lett.* **123**, 123601 (2019).
- [44] C. Li, G. Zhang, X. Z. Zhang, and Z. Song, Conventional quantum phase transition driven by a complex parameter in a non-Hermitian \mathcal{PT} -symmetric Ising model, *Phys. Rev. A* **90**, 012103 (2014).
- [45] X. Z. Zhang, L. Jin, and Z. Song, Dynamic magnetization in non-Hermitian quantum spin systems, *Phys. Rev. B* **101**, 224301 (2020).
- [46] Y.-G. Liu, L. Xu, and Z. Li, Quantum phase transition in a non-Hermitian XY spin chain with global complex transverse field, *J. Phys.: Condens. Matter* **33**, 295401 (2021).
- [47] L. Lenke, M. Mühlhauser, and K. P. Schmidt, High-order series expansion of non-Hermitian quantum spin models, *Phys. Rev. B* **104**, 195137 (2021).
- [48] S. Bi, Y. He, and P. Li, Ring-frustrated non-Hermitian XY model, *Phys. Lett. A* **395**, 127208 (2021).
- [49] K. Yamamoto, M. Nakagawa, M. Tezuka, M. Ueda, and N. Kawakami, Universal properties of dissipative Tomonaga-Luttinger liquids: Case study of a non-Hermitian XXZ spin chain, *Phys. Rev. B* **105**, 205125 (2022).
- [50] G. Chen, F. Song, and J. L. Lado, Topological spin excitations in non-Hermitian spin chains with a generalized kernel polynomial algorithm, *Phys. Rev. Lett.* **130**, 100401 (2023).
- [51] G. A. Starkov, M. V. Fistul, and I. M. Eremin, Formation of exceptional points in pseudo-Hermitian systems, *Phys. Rev. A* **108**, 022206 (2023).
- [52] G. A. Starkov, M. V. Fistul, and I. M. Eremin, Quantum phase transitions in non-Hermitian \mathcal{PT} -symmetric transverse-field Ising spin chains, *Ann. Phys. (NY)* **456**, 169268 (2023).
- [53] B. J. Ávila, C. Ventura-Velázquez, R. de J. León-Montiel, Y. N. Joglekar, and B. M. Rodríguez-Lara, \mathcal{PT} -symmetry from Lindblad dynamics in a linearized optomechanical system, *Sci. Rep.* **10**, 1761 (2020).
- [54] C. H. Liang, D. D. Scott, and Y. N. Joglekar, \mathcal{PT} restoration via increased loss and gain in the \mathcal{PT} -symmetric Aubry-André model, *Phys. Rev. A* **89**, 030102(R) (2014).
- [55] E. Lieb, T. Schultz, and D. Mattis, Two soluble models of an antiferromagnetic chain, *Ann. Phys. (NY)* **16**, 407 (1961).
- [56] P. Pfeuty, The one-dimensional Ising model with a transverse field, *Ann. Phys. (NY)* **57**, 79 (1970).
- [57] S. Sachdev, *Quantum Phase Transitions* (Cambridge University Press, Cambridge, 2009).
- [58] E. Fradkin, *Field Theories of Condensed Matter Physics* (Cambridge University Press, Cambridge, 2013).
- [59] F. Ruzicka, K. S. Agarwal, and Y. N. Joglekar, Conserved quantities, exceptional points, and antilinear symmetries in non-Hermitian systems, *J. Phys.: Conf. Ser.* **2038**, 012021 (2021).
- [60] N. Moiseyev and S. Friedland, Association of resonance states with the incomplete spectrum of finite complex-scaled Hamiltonian matrices, *Phys. Rev. A* **22**, 618 (1980).
- [61] S. Klaiman, U. Günther, and N. Moiseyev, Visualization of branch points in \mathcal{PT} -symmetric waveguides, *Phys. Rev. Lett.* **101**, 080402 (2008).